X-ray diffraction studies of expanded fluid mercury using synchrotron radiation

1998 J. Phys.: Condens. Matter 10 11405

(http://iopscience.iop.org/0953-8984/10/49/027)

J. Phys.: Condens. Matter **10** (1998) 11405–11417. Printed in the UK PII: S0953-8984(98)96502-X

X-ray diffraction studies of expanded fluid mercury using synchrotron radiation

K Tamura†, M Inui†, I Nakaso†, Y Oh'ishi†, K Funakoshi‡ and W Utsumi§

† Faculty of Integrated Arts and Sciences, Hiroshima University, Higashi-Hiroshima 739-8521, Japan

‡ Japan Synchrotron Radiation Research Institute, Kamigori 679-5198, Japan

§ The Japan Atomic Energy Research Institute, Kamigori 679-5198, Japan

Received 4 June 1998

Abstract. Energy-dispersive x-ray diffraction measurements using synchrotron radiation at SPring-8 for expanded fluid Hg were carried out over the wide density range from the liquid to the dense-vapour region including the metal–non-metal (M–NM) transition region. The density ranges from 13.6 to 1.9 g cm^{-3}. We developed a high-pressure vessel and a sapphire cell for the x-ray diffraction measurements under high temperature and pressure up to 1520 °C and 1765 bar. We obtained the structure factor $S(k)$ and the pair distribution functions $g(r)$. The density variations of the interatomic distance r_1 and coordination number N_1 obtained were discussed in relation to the M–NM transition in fluid Hg. It was found that the volume expansion of liquid Hg in the metallic region is not accompanied by a uniform increase of r_1, but is mainly caused by a decrease of N_1. When the transition region is crossed, the rate of decrease of N_1 becomes small and r_1 starts to elongate. We discussed some previous band calculations for expanded fluid Hg and concluded that it is essential for explaining the M–NM transition in liquid Hg to take the fluctuation of N_1 into account. When the density decreases down to the dense-vapour region, the first maxima of $g(r)$ are located at around 3.3–3.4 Å, which is close to the interatomic distance of Hg dimers.

1. Introduction

Liquid Hg is transformed into an insulating state when it is expanded up to the liquid–gas critical point (critical data for Hg [1]: $T_c = 1478$ °C, $p_c = 1673$ bar, $d_c = 5.8$ g cm^{-3}). Many investigations have been made over the last few decades, focused on the metal–non-metal (M–NM) transition in fluid Hg. The first indication of the M–NM transition was found in the electrical conductivity and thermopower data obtained by Hensel and Frank [2]. Figure 1 shows the density isochores plotted in the pressure–temperature plane [1]. Measurements of physical properties such as the electrical conductivity [3–5], thermopower [3, 6–8], Hall coefficient [9], optical reflectivity [10, 11], optical absorption coefficient [12, 13] and NMR [14] indicate that, as the density is reduced, the M–NM transition starts to occur at a density of about 9 g cm^{-3}. In relation to the transition, thermodynamic properties such as the equation of state [1, 2, 4, 5], sound velocity [15–18], sound attenuation [16, 17] and specific heat [19] were also investigated.

Theoretical attempts have been made to achieve an understanding of the nature of the M–NM transition. Several band-structure calculations have been carried out for the hypothetical forms of crystalline Hg in the low-density limit. The first calculation was by Devillers and Ross [20], who applied a pseudopotential method to calculate the energy

0953-8984/98/4911405+13$19.50

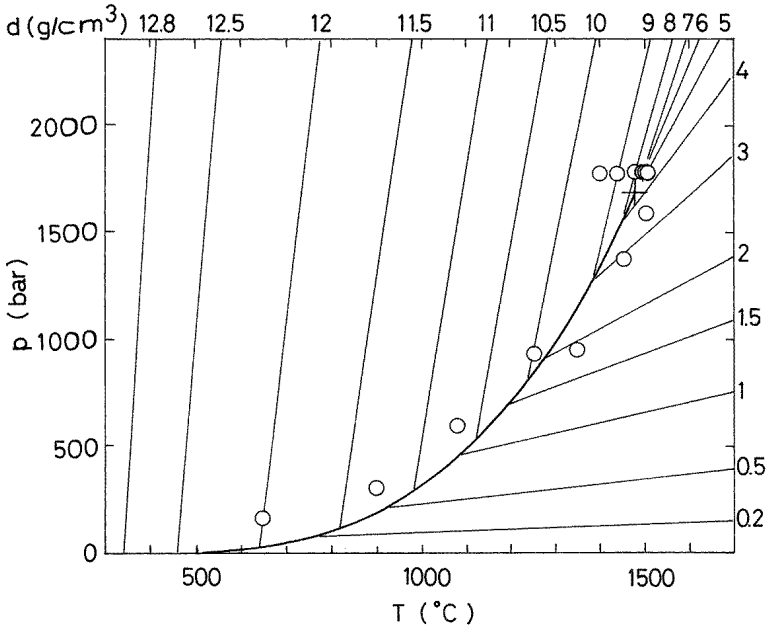

Figure 1. The density isochores plotted in the pressure–temperature plane [1]. A bold solid line indicates the saturated-vapour-pressure (SVP) curve and the cross shows the critical point (CP). Empty circles show the pressures and temperatures at which the present x-ray diffraction measurements were performed.

bands for crystalline Hg with expanded bcc, fcc and rhombohedral structures. For each structure, they obtained a band gap at about 8.5 g cm^{-3}. Band-structure calculations for such uniformly expanded crystalline Hg were carried out by many others [21, 22]. One alternative approach is that of Mattheis and Warren [23]. They assumed that the nearest-neighbour distance was constant, so the density variation in expanded fluid Hg was due entirely to the changes in the coordination number, and performed a series of augmented-plane-wave calculations for crystalline Hg with fcc (coordination number = 12), bcc (8), sc (6) and diamond (4) structures and a fixed nearest-neighbour distance. Their results showed a gradual development of the energy gap as the coordination number was reduced, although an increase of the lattice constant by 1% was necessary to fully open a gap in tetrahedral coordination.

These two different types of theoretical approach are illustrated in figure 2, which indicates how the structural change of fluid Hg takes place in the microscopic sense with volume expansion. The atomic arrangement indicated by (a) represents a uniform expansion in which the nearest-neighbour distance, r_1, increases and the coordination number, N_1, remains constant, which corresponds to the former approaches. The diagram (b), in contrast, shows an inhomogeneous expansion in which r_1 remains constant and N_1 decreases.

It is obvious that information on the atomic arrangement of expanded fluid Hg is quite important for the understanding of the M–NM transition. However, diffraction experiments for expanded fluid Hg are not easy, because the critical pressure is very high. Recently, Tamura and Hosokawa succeeded in measuring the x-ray diffraction using an in-house x-ray source for expanded liquid Hg in the metallic region and also up to the critical region [24–26]. They obtained information about the first-neighbour coordination—namely that r_1

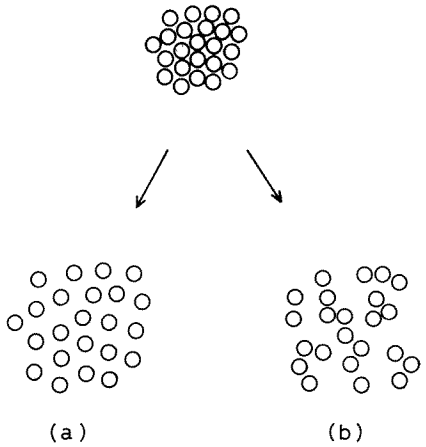

Figure 2. Schematic diagrams of how the structural change of fluid Hg takes place in the microscopic sense with volume expansion: (a) a uniform expansion in which the nearest-neighbour distance, r_1, increases and the coordination number, N_1, remains constant; and (b) an inhomogeneous expansion in which r_1 remains constant and N_1 decreases.

remains almost constant and N_1 decreases substantially and almost linearly with decreasing density in the metallic region, which corresponds to type (b) in figure 2. It is important to study how liquid Hg is expanded with further decrease of density, beyond the M–NM transition region, up to the dense-vapour region.

In this paper we present new results from x-ray diffraction measurements using synchrotron radiation, extending from the liquid to the dense-vapour region beyond the liquid–vapour critical point, which enable us to obtain more precise information about the atomic configuration.

2. Experiment

2.1. Constitution of the energy-dispersive diffractometer at SPring-8

We have performed energy-dispersive x-ray diffraction measurements for expanded fluid Hg using synchrotron radiation on the BL-04B1 at SPring-8. In the energy-dispersive method, white x-rays were used as the primary beam, and the scattered photons were detected and energy analysed by a solid-state detector (SSD). This technique has been employed in our in-house structural studies of expanded fluids [24–29]. The storage ring at SPring-8 was operated at 8 GeV with 20 mA during the present experiment. White x-rays were generated through the bending magnet, ranging in energy up to 150 keV. The size of the x-ray beam was made smaller, down to 0.2×0.2 mm^2, using the horizontal and vertical tungsten slits in the upper stream. The beam was directly introduced into the high-pressure vessel through the Be window of the vessel which is illustrated in the following section. As a result, the background noise due to the secondary x-rays in the hutch was substantially reduced.

In the hutch we have a high-pressure- and high-temperature-generation system and an energy-dispersive x-ray diffractometer. The former system includes a gas compressor, a high-pressure vessel, a thermocontroller and a chiller. The diffractometer is composed of a goniometer, adjustable stages and a pure Ge SSD. A horizontal goniometer system was adopted, in which an x-ray source and a detector were set in a horizontal plane. The

scattered x-rays were detected by the SSD, which was rotated around the vertical axis of the goniometer, and connected with a multichannel pulse-height analyser (MCA). Energy-dispersive measurements were performed at a fixed scattering angle 2θ and repeated at different angles in order to cover a sufficiently wide range of scattering wavenumber k, $k = (4\pi(\sin\theta)/hc)E$ (E: photon energy; h: Planck's constant; c: velocity of light). The position of the fluid sample contained in the sapphire cell, the details of which are described in the following section, was adjusted to be on the central axis of the goniometer. The high-pressure vessel was placed on the goniometer. In the present experiment, transmission geometry was employed.

Since helium gas was used as a pressure-transmitting medium, most of these pieces of equipment were placed in the small room surrounded by a protective wall which was built inside the hutch.

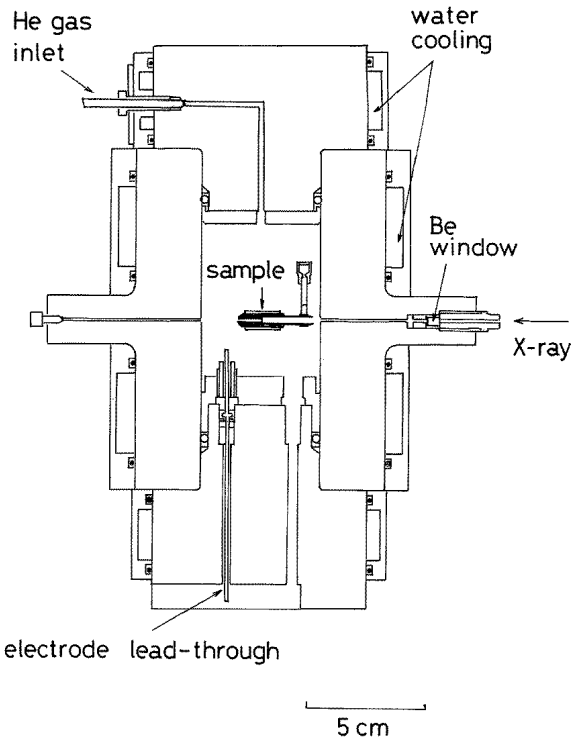

Figure 3. A side view of the high-pressure vessel used for x-ray diffraction studies.

2.2. The high-pressure vessel

The experimental conditions of high temperatures, up to 1520 °C, and high pressures, up to 1765 bar, were achieved with an internally heated high-pressure vessel made of a super-high-tension steel. Figure 3 shows the side view of the high-pressure vessel which was constructed of a main cylinder with an inner diameter of 50 mm, an outer diameter of 105 mm and a length of 140 mm, and two flanges with thicknesses of 43 and 49 mm. These flanges were supported by a press-frame when the high-pressure gas was introduced into the vessel. The sample was located on the central axis of the high-pressure vessel and

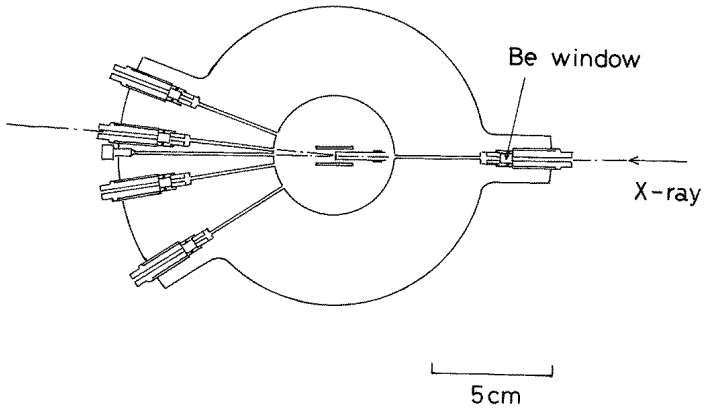

Figure 4. A top view of the high-pressure vessel used for x-ray diffraction studies.

the alumina discs were used for holding the sapphire cell. The primary and scattered x-ray beams passed through Be windows of thickness 5 mm and diameter 4 mm. Each of the Be windows was supported by the flat area of a back-up screw. Figure 4 shows the top view of the high-pressure vessel. As seen in the figure, there were five Be windows, one of which was for the primary x-ray beam and the rest for the scattered ones. The windows for the scattered x-ray beams were located at 2θ-values of 5, 10, 20 and 33°. The electrodes for the heaters and thermocouples were brought out of the vessel through the lower flange, where Bridgman-type high-pressure seals were used. The vessel was pressurized by high-purity-grade (99.9999%) He gas which has a low absorption constant for x-rays in the energy range of the present experiment. Pressures were measured with a Heise gauge, having an accuracy of ± 3 bar. Water cooling jackets were placed around the outside of the vessel.

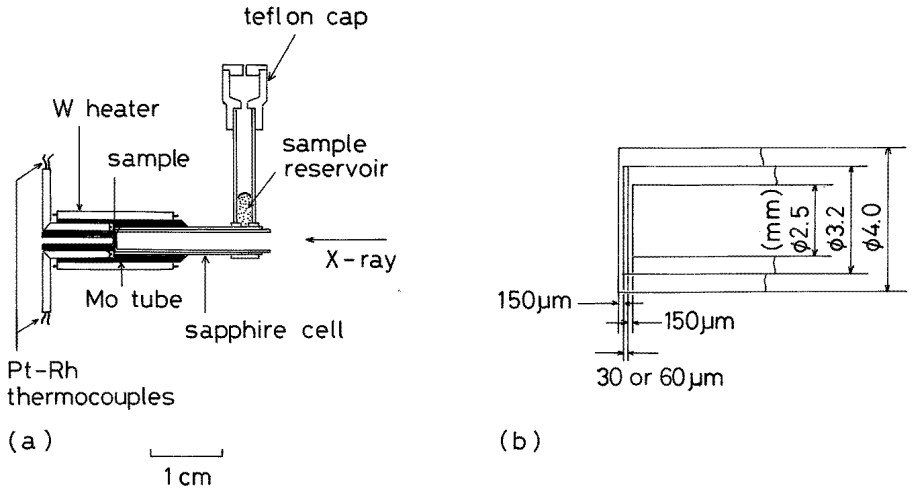

Figure 5. (a) The construction of the sapphire cell used for the present x-ray diffraction studies of expanded fluid Hg. (b) Details of the sample space shown on an enlarged scale.

2.3. The sample cell

Expanded fluid Hg must be contained in a cell made of a special material, which is transparent to x-rays and resistant to chemical corrosion by hot fluid Hg. A single-crystal sapphire cell was developed for this purpose, the details of which are illustrated in figure 5(a) and described in the literature [29]. The construction around the fluid sample is shown in figure 5(b) on an enlarged scale. A closed-end sapphire tube with an inner diameter of 2.5 mm, an outer diameter of 3.2 mm and a length of 21.4 mm was put into another closed-end tube with an inner diameter of 3.2 mm, an outer diameter of 4.0 mm and a length of 20.5 mm. The sapphire components were connected with a high-temperature glaze providing a uniform gap between the closed ends of the tubes. The thickness of the closed end of each tube through which the x-ray passed was 150 μm, and the gap was 30 or 60 μm.

In measuring x-ray diffraction from the fluid sample contained in the sample cell, the problem was that of how to distinguish the strong diffraction from the sapphire cell. This was overcome by the assembly of the cell [29].

The cell was heated by a heating element made of W wire with a diameter of 0.4 mm. The W heater was set around a Mo tube. Since a slit was made on the left-hand side of the Mo tube, diffracted x-rays were able to go out through it. The temperature of the sample was measured by two Pt–30% Rh:Pt–6% Rh thermocouples which were located in the holes of the Mo tube and were in close contact with the wall of the closed end of the

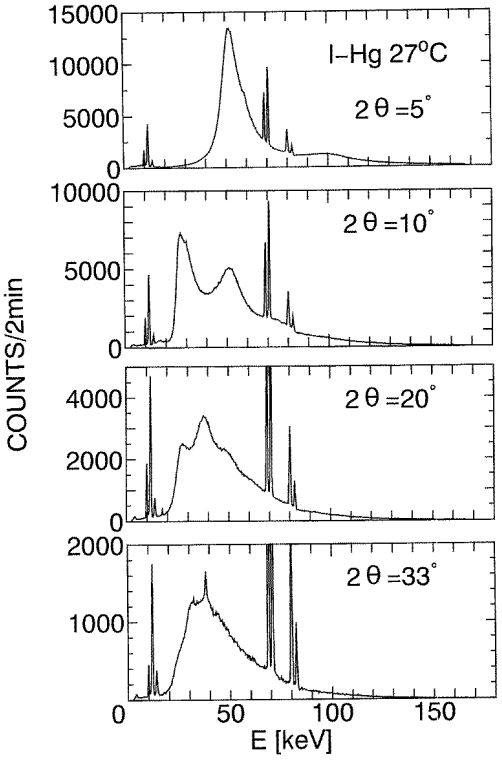

Figure 6. The raw spectra obtained at different angle settings for liquid Hg under normal conditions.

outer sapphire tube. The cell and the heaters were supported by alumina discs. Special care was taken to construct the alumina discs such that the sample was precisely positioned on the central axis of the vessel. The space between the alumina discs and the inner wall of the vessel was filled with alumina powder to obtain good thermal insulation and to prevent convection of the compressed He gas.

The procedure for filling the sample space between the closed ends of the cell with fluid Hg is described in the literature [26]. The temperature of the reservoir was maintained near room temperature. Pressure balance between the compressed fluid Hg and the He gas was achieved through a small hole in the upper part of the Teflon cap. The purity of the Hg sample was 99.9999%.

2.4. X-ray diffraction measurement and data analysis

The x-ray photons diffracted from expanded fluid Hg at high temperatures and pressures were collected at 2θ-values of 5, 10, 20 and 33°. Figure 6 shows the raw spectra of liquid Hg under normal conditions obtained at different angle settings. The spectrum used for the analysis was in the energy region 16–60 keV because the strong fluorescence peak appeared at higher energy, so difficulties arose in the present analysis.

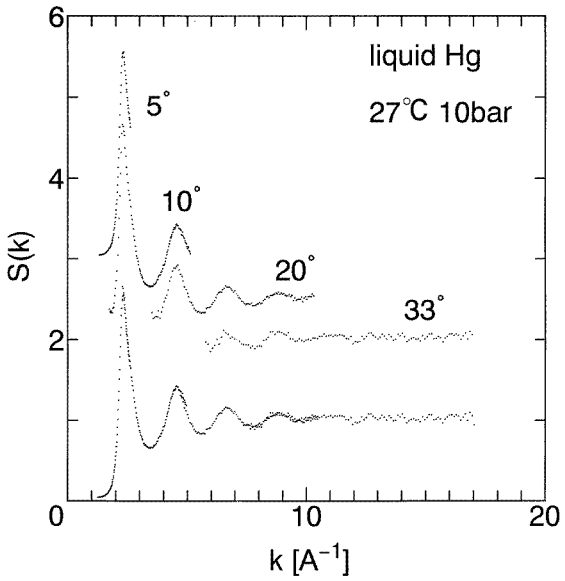

Figure 7. $S(k)$ data obtained at different angle settings for liquid Hg at 27 °C and 10 bar. The lowest curve shows the total $S(k)$.

In order to obtain $S(k)$ for expanded fluid Hg from the experimental scattering intensity, several data corrections had to be made such as taking account of the escape peak of the detector, the energy spectrum of the primary x-ray beam, the energy dependence of the polarization of the primary beam, the absorption by the sapphire cell, the compressed He gas, the Be windows and the fluid Hg itself, and finally Compton scattering from the fluid Hg and the sapphire cell. The details of the data analysis have been described in the literature [24, 30]. Figure 7 shows the $S(k)$ data for different angle settings for liquid Hg at 27 °C and 10 bar which have an excellent consistency in the same k-region.

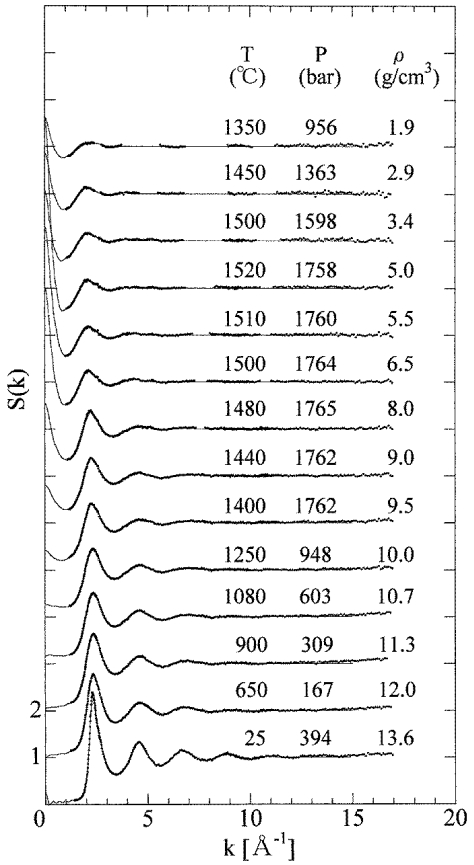

Figure 8. The structure factor $S(k)$ for expanded fluid Hg in the temperature and pressure ranges up to 1520 °C and 1765 bar along the saturated-vapour-pressure curve. Temperature, pressure and density are indicated on the upper right-hand side of each of the data plots. The dots represent the experimental data and the full curves show the Fourier transforms of the $g(r)$ in figure 9.

3. Results

We have carried out x-ray diffraction measurements for expanded fluid Hg in the temperature and pressure ranges up to 1520 °C and 1765 bar along the saturated-vapour-pressure curve and with densities ranging from 13.6 to 1.9 g cm^{-3}. Empty circles in figure 1 show the temperatures and pressures at which the present measurements were performed. Figure 8 shows the $S(k)$ for expanded fluid Hg for the different temperatures and pressures obtained using the cell with the sample thickness of 60 μm. Dots represent the experimental data and the full curves show the Fourier transforms of the $g(r)$ in figure 9. $S(k)$ at 25 °C and 364 bar is in good agreement with previous data obtained under normal conditions by the usual angle-dispersive method [31].

The characteristic feature of the temperature and pressure variations of $S(k)$ is that the oscillation damps and the peak width becomes broad with increasing temperature and pressure, or with decreasing density.

Figure 9 shows the $g(r)$ curves, the Fourier transforms of $S(k)$, for fluid Hg. The

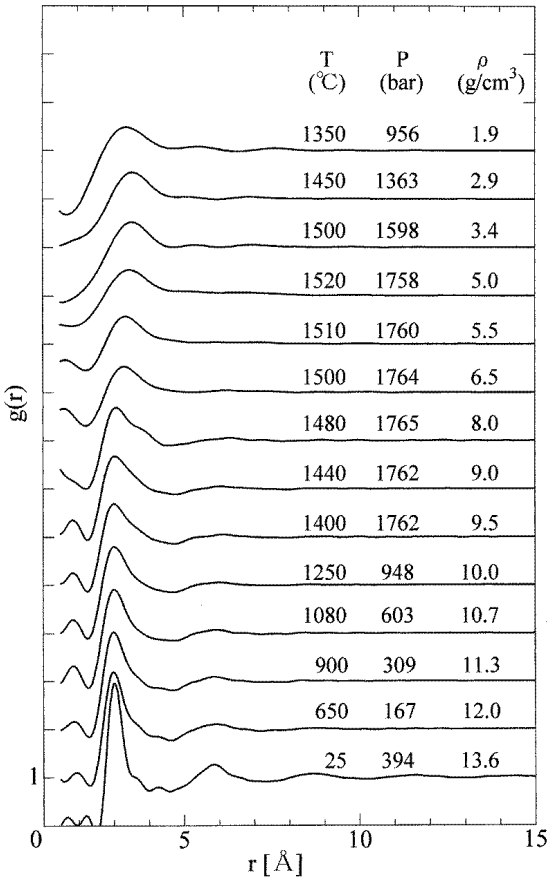

Figure 9. Pair distribution functions $g(r)$ for expanded fluid Hg. Temperature, pressure and density are indicated on the upper right-hand side of each of the data plots.

transform of the $S(k)$ function requires data from $k = 0$ to ∞. A lack of exact data for small values of k is, however, not so serious because the function $k(S(k)-1)$ is very small in this region. The values of $S(k)$ in the small-k region between 0 and 1.0 Å^{-1} were estimated by interpolating the values of $S(0)$ and $S(k)$ above 1.0 Å^{-1}, where the values of $S(0)$ were calculated using the experimentally obtained isothermal compressibility of expanded fluid Hg [1, 4].

The data for $g(r)$ at 25 °C and 394 bar have several characteristic features; the first peak has an asymmetric shape, the first minimum is flat over the wide region from 4 to 5 Å and the second peak is rather small. The data for $g(r)$ at 25 °C and 394 bar are in excellent agreement with the previous data for the normal condition [31]. With increasing temperature and pressure, with decreasing density, the long-range oscillation of $g(r)$ diminishes. The broadening of the first peak gradually occurs but no remarkable change of the peak position is observed and the asymmetry of the first peak clearly remains even at high temperatures and pressures up to 1480 °C and 1765 bar with a density of 8.0 g cm^{-3}. It should be noticed that the shape and the position of first peak changes dramatically when the density decreases further and the dense-vapour region is approached. The second peak damps rapidly with increasing temperature and pressure.

4. Discussion

It is not easy to obtain a definite coordination number, N_1, from the diffusive and broad $g(r)$ pattern of the non-crystalline state. Since there is an overlap between the first- and second-neighbour peaks, experimental values of N_1 depend on the method employed to define and to integrate the first-neighbour peak. However, variations of N_1 as a function of temperature, pressure or density can be determined with more reliability as long as a consistent definition of N_1 is used. We employed two different methods to define and to integrate the first-neighbour peak [32]. The first (method A) is the method of integrating $4\pi r^2\rho_0 g(r)$ up to the maximum position of $g(r)$, r_1, and taking twice the integral, where ρ_0 denotes the average number density of Hg. The second (method B) is a special method for taking the asymmetry of the first-neighbour peak into account. In method B, a tangential straight line is drawn from the first-peak position, r_{max}, towards the first minimum of $4\pi r^2\rho_0 g(r)$. The area of the triangle below the tangent line is regarded as that due to the penetration of the second neighbours, and is subtracted.

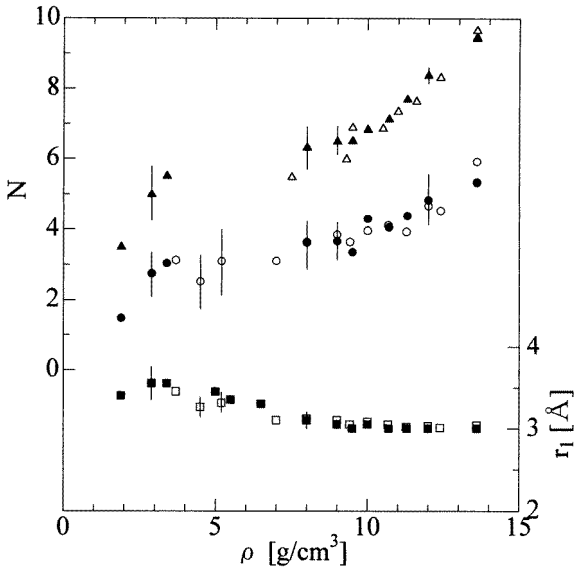

Figure 10. The coordination number N_1 and the nearest-neighbour distance r_1 of expanded fluid Hg as functions of the density. Circles and triangles denote N_1 obtained using methods A and B, respectively (see the text). Squares show the variation of r_1. Empty and full symbols indicate the data obtained using the cells with the sample thicknesses of 30 and 60 μm, respectively.

The coordination numbers N_1 obtained by these calculations are plotted in figure 10 as a function of density. The nearest-neighbour distance r_1 is also shown as a function of density at the bottom of figure 10. In the figure we plot the data obtained by using the cells with the sample thicknesses of 30 and 60 μm. The value of r_1 at 25 °C and 394 bar is 3.04 Å—slightly longer than that of the crystal with the rhombohedral form, 3.00 Å [33]. As is clearly seen in figure 10, N_1 decreases substantially and linearly with decreasing density in the metallic region, whatever method is employed. In contrast, r_1 in the metallic region remains almost unchanged with decreasing density within the accuracy of the present experiment. From these results we can conclude that the volume expansion of liquid Hg

in the metallic region is not of the type of 'a uniform expansion with a fixed coordination number' illustrated in figure 2(a), but is caused by 'a decrease of coordination number with a fixed nearest-neighbour distance' shown in figure 2(b). The atomic arrangement of metallic liquid Hg would be changed with decreasing density essentially in the way that Hg atoms are taken away one by one from the random array with a constant nearest-neighbour distance.

When the M–NM transition is approached from the high-density side, i.e., at around 9–10 g cm^{-3}, however, another deviation from the linear plots of N_1 emerges. In addition, r_1 starts to slightly increase. When the dense vapour is approached with further decreasing density, r_1 strongly increases. The value of r_1 seems to approach the interatomic distance 3.3–3.4 Å of Hg dimers in the rarefied vapour, obtained by the optical measurement [34].

As is well known, the M–NM transition for liquid Hg is expected at low densities when the 6s and 6p bands no longer overlap. In the case of liquid, the sharpness of the transition would be relaxed by the density fluctuations and the loss of the long-range order. According to Mott [35], the band structure for a hypothetical form of crystalline Hg in which the lattice parameter is gradually increased would produce initially a minimum in the density of states (DOS) near the Fermi energy E_F and eventually a band gap. Mott suggested that the general features of this crystalline model for Hg would survive in the liquid.

Several band-structure calculations were carried out for the hypothetical forms of crystalline Hg with uniformly expanded lattice constants in the low-density limit. The first calculation was by Devillers and Ross [20], who applied the pseudopotential method to calculate the energy bands for crystalline Hg with bcc, fcc and rhombohedral structures. For each structure, they obtained a band gap at about 8.5 g cm^{-3}, in general agreement with the transport data. Overhof *et al* [21] carried out relativistic Korringa–Kohn–Rostoker calculations for expanded fcc and sc Hg and found that fcc Hg becomes semiconducting at $\rho = 9.3$ g cm^{-3} while sc Hg remains a metal until $\rho = 5.5$ g cm^{-3}. A similar dependence on crystal structure was obtained by Fritzson and Berggren [22], who carried out pseudopotential calculations for expanded fcc, bcc and sc Hg and found that band gaps open up at $\rho = 6.5$ g cm^{-3} for fcc, 5.5 g cm^{-3} for bcc and 4 g cm^{-3} for sc Hg.

These theoretical models and calculations were based on the uniform expansion of the lattice parameter. The present experimental results for fluid Hg, however, are definitely different. One of the approaches whose principle was consistent with the present experimental results was that of Mattheis and Warren [23]. They assumed that the nearest-neighbour distance was constant, so the density variation in expanded fluid Hg was due entirely to the changes in the coordination number. They performed a series of augmented-plane-wave calculations for crystalline Hg with fcc, bcc, sc and diamond structures with a fixed nearest-neighbour distance. They found that the trend of the density dependence of the theoretically calculated DOS with the 6s character is in good agreement with that of the Knight shift in the density range down to about 9.5 g cm^{-3} by assuming that N_1 for liquid Hg near the triple point was 10, and linearly decreased with decreasing density. However, their hypothetical crystal with diamond structure with $N_1 = 4$, which corresponds to $\rho = 5.4$ g cm^{-3} according to the interpretation of Warren and Hensel [36] using revised density data, indicates a semimetallic DOS, and it was found necessary to increase the lattice constant by 1% to fully open a gap.

Franz [37] proposed a model that produces a real gap at the correct density of 9 g cm^{-3}. The model was also based on the assumption of a linear decrease in average coordination number with decreasing density, but in addition it takes into account the fact that the actual local coordination numbers would be distributed randomly over a range of values around the

mean value. The calculation was performed using a standard single-particle Green's function method with a Bethe lattice to represent the disordered system and a Monte Carlo technique to produce the random local environment. The density of the percolation threshold or the M–NM transition density was obtained as about 9 g cm^{-3}. The model seems to strongly suggest that the fluctuation of the coordination number must play an important role in the M–NM transition in fluid Hg.

Recently, Kresse and Hafner [38] made a theoretical investigation of the density variation of the structural and electronic properties of fluid Hg using an *ab initio* density-functional molecular dynamics method. They found that a single-particle gap between the 6s and 6p bands opens at a density of about 8.8 g cm^{-3}, and that both disorder-induced localization and many-body effects might be unimportant. They could reproduce well the manner of the volume expansion in fluid Hg, which results not in an increase of the mean interatomic distance r_1, but in a decrease of the average coordination number N_1. In addition, the asymmetry of the first peak in $g(r)$ was evidently reproduced in their calculated results over the whole density range. However, the experimental result of the small shift of r_1 to the larger distance when the density decreases to less than 9 g cm^{-3} could not be reproduced in their calculation.

We have concentrated so far on discussing the density variation of just the first-neighbour coordination in relation to the M–NM transition in fluid Hg. However, we can see in figure 9 that more information is included in the $g(r)$ data. The asymmetry of the first peak clearly remains even at high temperatures and pressures up to 1480 °C and 1765 bar with a density of 8.0 g cm^{-3}. The asymmetry may suggest that there exist two sites in the first coordination. The second peak damps rapidly with increasing temperature and pressure but the maximum position gradually shifts to larger distance with decreasing density. The changes of the coordination number and the position of these sites in the first neighbour must play an important role in the M–NM transition.

In the dense-vapour region, we can see in figure 9 that the first peak, the shape of which is dramatically changed compared with those in the metallic region, remains clear but the second-neighbour correlation is almost lost. This suggests that small clusters such as Hg dimers ($N_1 = 1$), triangles ($N_1 = 2$), or tetrahedrons ($N_1 = 3$) might exist near the critical range. In order to get information on the cluster formation in fluid Hg, it is very important to make more precise x-ray diffraction measurements in the low-density region. Moreover, computer simulation investigations with large system sizes and precise analyses can also provide this information.

Acknowledgments

The authors are grateful to Professor S Hosokawa for valuable discussions and Dr Y Sakaguchi for technical assistance. Kobe Steel Company Limited, High Pressure System Company Limited and Rigaku Company Limited are acknowledged for technical support during the present experiment. This work was partly supported by a Grant-in-Aid for Scientific Research Fund from the Ministry of Education, Science, Sports and Culture of Japan, and Toray Science Foundation.

References

[1] Gözlaff W, Schönherr G and Hensel F 1988 *Z. Phys. Chem., NF* **156** 219
Gözlaff W 1988 *PhD Thesis* University of Marburg
[2] Hensel F and Frank E U 1966 *Ber. Bunsenges. Phys. Chem.* **70** 1154

[3] Schmutzler R W and Hensel F 1972 *Ber. Bunsenges. Phys. Chem.* **76** 53
[4] Schönherr G, Schmutzler R W and Hensel F 1976 *Phil. Mag.* B **40** 411
[5] Yao M and Endo H 1982 *J. Phys. Soc. Japan* **51** 966
[6] Duckers L J and Ross R G 1972 *Phys. Lett.* **38A** 291
[7] Neale F E and Cusack N E 1979 *J. Phys. F: Met. Phys.* **9** 85
[8] Yao M and Endo H 1982 *J. Phys. Soc. Japan* **51** 1504
[9] Even U and Jortner J 1972 *Phil. Mag.* **25** 715
Even U and Jortner J 1973 *Phys. Rev.* B **8** 2536
[10] Ikezi H, Schwarzenegger K, Simons A L, Passner A L and McCall S L 1978 *Phys. Rev.* B **18** 2494
[11] Hefner W, Schmutzler R W and Hensel F 1980 *J. Physique Coll.* **41** C8 62
[12] Uchtmann H and Hensel F 1975 *Phys. Lett.* **53A** 239
Uchtmann H, Brusius U, Yao M and Hensel F 1988 *Z. Phys. Chem., NF* **156** 151
[13] Yao M, Takehana K and Endo H 1993 *J. Non-Cryst. Solids* **156–158** 807
[14] El-Hanany U and Warren W W Jr 1975 *Phys. Rev. Lett.* **34** 1276
[15] Suzuki K, Inutake M, Fujiwaka S, Yao M and Endo H 1980 *J. Physique Coll.* **41** C8 66
[16] Kozhevnikov V, Arnold D, Grodzinskii E and Naurzakov S 1996 *J. Non-Cryst. Solids* **205–207** 256
[17] Yao M, Okada K, Aoki T and Endo H 1996 *J. Non-Cryst. Solids* **205–207** 274
[18] Dladla B S, Pilgrim W-C and Hensel F 1997 *Z. Phys. Chem.* **199** 295
[19] Levin M and Schmutzler R W 1984 *J. Non-Cryst. Solids* **61+62** 83
[20] Devillers M A C and Ross R G 1975 *J. Phys. F: Met. Phys.* **5** 73
[21] Overhof H, Uchtmann H and Hensel F 1976 *J. Phys. F: Met. Phys.* **6** 523
[22] Fritzson P and Berggren K-F 1976 *Solid State Commun.* **19** 385
[23] Mattheis L F and Warren W W Jr 1977 *Phys. Rev.* B **16** 624
[24] Hosokawa S, Matsuoka T and Tamura K 1991 *J. Phys.: Condens. Matter* **3** 4443
[25] Tamura K and Hosokawa S 1991 *J. Physique Coll.* IV **1** C5 39
[26] Tamura K and Hosokawa S 1998 *Phys. Rev.* B **58** 9030
[27] Tamura K 1990 *J. Non-Cryst. Solids* **117+118** 450
[28] Tamura K and Hosokawa S 1992 *Ber. Bunsenges. Phys. Chem.* **96** 681
[29] Tamura K, Inui M and Hosokawa S 1998 *Rev. Sci. Instrum.* at press
[30] Nishikawa K and Iijima T 1984 *Bull. Chem. Soc. Japan* **57** 1750
[31] Bosio L, Cortes R and Segaud C 1979 *J. Chem. Phys.* **71** 3595
[32] Pings C J 1968 *Physics of Simple Liquids* ed H N V Temperley, J S Rowlinson and G S Rushbrooke (Amsterdam: North-Holland) pp 405–411
[33] Mehl R F and Barrett C S 1930 *Trans. AIME* **89** 575
[34] Winans J G and Heitz M P 1952 *Z. Phys.* **133** 291
Winans J G and Heitz M P 1953 *Z. Phys.* **135** 406
[35] Mott N F 1966 *Phil. Mag.* **13** 989
Mott N F 1967 *Adv. Phys.* **16** 49
Mott N F 1972 *Phil. Mag.* **26** 505
[36] Warren W W Jr and Hensel F 1982 *Phys. Rev.* B **26** 5980
[37] Franz J R 1986 *Phys. Rev. Lett.* **57** 889
[38] Kresse G and Hafner J 1997 *Phys. Rev.* B **55** 7539